Molecular Therapy
Nucleic Acids
Original Article

Fine-tuning miR-21 expression and inhibition of EMT in breast cancer cells using aromatic-neomycin derivatives

Arpita Ghosh,[1,2] Nihar Ranjan,[3] Liuwei Jiang,[3] Asgar Hussain Ansari,[1,2] Natalya Degyatoreva,[4] Shivaksh Ahluwalia,[1,5] Dev P. Arya,[3,4] and Souvik Maiti[1,2]

[1]CSIR-Institute of Genomics & Integrative Biology, Mathura Road, Delhi 110025, India; [2]Academy of Scientific & Innovative Research, CSIR- Human Resource Development Centre (CSIR-HRDC) Campus, Sector 19, Kamla Nehru Nagar, Ghaziabad 201 002, Uttar Pradesh, India; [3]Department of Chemistry, Clemson University, Clemson, SC 29634, USA; [4]NUBAD LLC, Greenville, SC 29605, USA; [5]Kusuma School of Biological Sciences, Indian Institute of Technology Delhi, New Delhi, Delhi 110016, India

MicroRNAs (miRs) are a class of endogenously expressed non-coding RNAs that negatively regulate gene expression within cells and participate in maintaining cellular homeostasis. By targeting 3′ UTRs of target genes, individual miRs can control a wide array of gene expressions. Previous research has shed light upon the fact that aberrantly expressed miRs within cells can pertain to diseased conditions, such as cancer. Malignancies caused due to miRs are because of the high expression of onco-miRs or feeble expression of tumor-suppressing miRs. Studies have also shown miRs to engage in epithelial to mesenchymal transition (EMT), which allows cancer cells to become more invasive and metastasize. miR-21 is an onco-miR highly expressed in breast cancer cells and targets protein PTEN, which abrogates EMT. Therefore, we discuss an approach where in-house-developed peptidic amino sugar molecules have been used to target pre-miR-21 to inhibit miR-21 biogenesis, and hence antagonize its tumor-causing effect and inhibit EMT. Our study shows that small-molecule-based fine-tuning of miR expression can cause genotypic as well as phenotypic changes and also reinstates the potential and importance of nucleic acid therapeutics.

INTRODUCTION

Cancer is a complex disease that can progress to different levels of severity. The outgrowth of a tumor in the body from one tissue to another distant tissue occurs by entering into the blood and lymphatic circulation and marks the most fatal stage of the disease. Mortality caused due to cancer to date is about 90% around the world,[1] and it is mostly due to the phenomena occurring at the later stages, such as epithelial to mesenchymal transition (EMT) and metastases.[2–4] The understanding of the molecular machinery behind metastases is very limited and thus leads to a lack of effective therapeutic methods to intervene. EMT is a process that is also found during embryogenesis,[5,6] where it gives rise to the diverse organ systems from the different lineage of cells. In cancer, EMT is a hallmark for the beginning of metastases.[7] The primary characteristics of an epithelial cell are adhesion, attachment to the basement membrane, cell to cell contact, apicobasal polarity, and innervated, non-vascular nature. Due to the onset of EMT, a cascade of signaling pathways is triggered that gives rise to stepwise changes in the epithelial cells that cause loss of its epithelial characteristics. Upon this transition, the cells acquire lamellipodia- and filopodia-like features, which gives them migratory and motility behavior, which is followed by extravasation and angiogenesis. The tumor cells enter into the circulatory system and further spreads to distant sites, giving rise to secondary and tertiary tumors; pathologically the most chronic state of cancer.[4,7,8]

The molecular determinants to understand the phenomena of EMT and metastases are still under study, but its progression can be triggered by differential expression of several microRNAs (miRs) in various cancers.[9,10] For example, low expression of miR-335 and miR-126 leads to metastases,[11] whereas elevated levels of miR-21[12,13] or miR-10b[14] have been reported to cause the same. MicroRNAs are endogenously expressed within cells and belong to the small non-coding class of RNA. They are ~22 nucleotides in length and affect the stability of RNA and translation negatively, thereby controlling gene expression.[15] The maturation of miR happens in various steps where initially a several kb long primary transcript (pri-miR) is transcribed from the DNA by RNA polymerase (Pol) II or Pol III enzyme. The pri-miR is then processed by Drosha, a nuclear endonuclease to generate the precursor microRNA (pre-miR) which is around 70–80 bp long. The pre-miR is exported to the cytoplasm from the nucleus by an Exportin complex where further trimming happens by the cytoplasmic RNAse III Dicer to form the mature miR sequence of 22–25 bp in size. Mature miRs are loaded onto the RISC complex by the Ago protein where the strand selection happens, and when they exhibit their function by

Received 15 May 2020; accepted 17 December 2021;
https://doi.org/10.1016/j.omtn.2021.12.027.

Correspondence: CSIR-Institute of Genomics & Integrative Biology, New Delhi, Delhi 110025, India.
E-mail: souvik@igib.res.in
Correspondence: Department of Chemistry, Clemson University, Clemson, SC 29634, USA.
E-mail: dparya@clemson.edu

recognizing and binding to the 3′ untranslated regions (UTRs) of their target mRNAs.[16] Partial complementarity to the target leads to transcriptional stalling, whereas complete binding causes mRNA degradation.[17] Since the mature miRs can also imperfectly bind to their targets, it opens up the possibility of one single miR to regulate multiple genes.[18,19] This ability of the miR to modulate gene expression gives rise to various clinical conditions when they are aberrantly expressed, and therefore opens up new avenues for prognosis.

MicroRNA anomalous expression is related to a plethora of diseases, such as leukemia,[20] cardiac hypertrophy,[21,22] diabetes,[23,24]Alzheimer's disease,[25,26] and hepatic viral infection.[27,28] The expression of miRs in blood has also been harnessed as a potential biomarker for diseases.[29] Atypical expression of miRs in cancer has also been reported. miRs that target tumor-suppressing genes, and are very highly expressed in cancer cells are termed as onco-miRs.[30–32] While certain miRs that target the oncogenes which promote cancer, and are lowly expressed within cells, is known as tumor-suppressing miRs.[33–36] miR-21 is one such onco-miR[37–39] whose expression levels are very high in breast cancer cells[40] and is known to target proteins, such as PDCD4,[40,41] PTEN,[40,42] and Bcl2, all of which have tumor suppression potential. Out of these targets, loss of function of PTEN is known to trigger EMT. The EMT is observed by the expression of distinct cellular markers, such as E-cadherin, N-cadherin, vimentin, Snail, Slug, and Zeb-1, to name a few.[4,6,7,42] The mesenchymal characteristic of a cell is marked by upregulation of transcription factors, such as Snail, Slug, and Zeb-1.[4,7] Snail is one of the early markers to get expressed during the onset of EMT by the PI3K/Akt pathway. PTEN expression impedes the PI3K/Akt pathway.[43] miR-21 overexpression in cancer inhibits PTEN, which is followed by the activation of Snail, which further initiates a downstream cascade of pathways that determine mesenchymal transition of a cell through the expression of vimentin. In cancer caused due to miRs, various therapeutic strategies have been designed. Initial studies involved the administration of antisense miR complementary to the mature miR sequence to reduce miR expression levels.[44–47] Although the strategy was effective, certain constraints, such as less stability within the cellular environment, cellular delivery, and uptake, limited its therapeutic potential. Furthermore, modified and more stable anti-miRs were also designed to counter the low stability,[48] but the delivery issue remained a hurdle. Subsequently, small molecules came up as promising candidates for therapeutic application against miRs involved in cancer.[49] Their easy delivery and uptake with lower diffusion and dissociation rates within cells gave them an upper hand over antisense miRs. Added advantages, such as longer stability and minimal toxicity[50–52] made them more suitable. Small molecules bind to the bulged loop structure of the pre-miR sequence and competes with Dicer for binding, thereby hindering it to process the miR into mature form. Our lab, has developed an in-house library of aminoglycoside conjugates targeting miR-21 where small peptides and aromatic units are conjugated to different aminoglycosides. We have reported the synthesis and RNA binding of a diverse series of aminoglycoside derivatives.[48,50,52–63] A number of these studies identified promising RNA binders where aromatic units were covalently attached to the aminoglycoside. Here in this study, we report the comparative cellular studies of 13 aromatic-neomycin conjugates (Figure 1) identified via a miR-21 displacement assay using F-neo, a reporter molecule.[57] Following the F-neo-based screening of the molecules, they were further tested *in cellulo* to evaluate its potential in reducing miR-21 effects. Promising small-molecule candidates that could reduce mir-21 levels *in cellulo* were further studied for binding, and were assessed for their ability to elevate the target protein levels of miR-21. Encouraging results from the above led us to study the downstream processes of the proteins, such as effect on proliferation and migration of the cells and also EMT. Our study shows that the in-house-developed molecules can effectively inhibit aberrant expression of miR-21 and also hinder EMT, thereby acting as a gatekeeper for metastases in cancer. The results open a wide door for pharmacologists and clinicians to explore and harness the potential of such small molecules.

RESULTS

Efficacy of aromatic-neo small molecules in downregulating miR-21 transcript levels

The advantage of the small molecule toward cancer therapeutics is due to the ease of its cellular uptake. Treatment of these molecules without any transfecting agent makes them effective enough within cells. For aromatic-neo conjugates, they could target miR-21 at its precursor stage leading to a stall in its maturation. We, therefore, checked for the mature miR-21 levels within MCF-7 breast cancer cells 48 h post-treatment of molecules at 5 μM concentration by qRT-PCR. Neomycin and neomycin TFA along with untreated cells were experimental controls and streptomycin (treated at 5 μM concentration) and locked nucleic acid (LNA)-modified antimiR-21 (transfected at 50 nM concentration) served as positive controls. We found that DPA 1171 and DPA 560 were highly effective in curbing miR-21 levels, even more than the positive controls used (as shown in Figure 2A). For both molecules that effectively suppressed miR-21, we performed treatment in an increasing concentration gradient to see their effect on the mature transcript. qRT-PCR was carried out 48 h post-treatment of DPA 560 and DPA 1171, which indicated a gradual decrease in miR-21 levels upon the incremental dosage of both molecules (Figures 2B and 2C). In the case of DPA 560, considerable downregulation of miR-21 was achieved at 0.5 μM concentration, and a further gradual decrease was found with each increasing concentration, showing a maximum effect at 10 μM concentration. The effect in miR-21 knockdown with DPA 1171 was more prominent at 2.5 μM and was maximally achieved at 10 μM. Depending on the dose-dependent qRT-PCR analysis, we found DPA 560 to downregulate miR-21 more effectively even at lower concentrations, and the maximum effect obtained was also more than DPA 1171. We further monitored the effect of DPA 560 on the pre-miR-21 and mature miR-21 in MCF-7 cells along with, MDA-MB-231 (an invasive breast cancer cell line) and HeLa (a cervical cancer cell line) cells via qRT-PCR. We found no effect on the pre-miR-21 levels, whereas across all the three cell lines, these molecules could effectively downregulate mature miR-21 (Figures 2D, S1A, and S1B). Global profiling for miRs was performed in MCF-7 cells upon treatment with the most effective DPA 560 molecule. Expression analysis of 47 differentially expressed

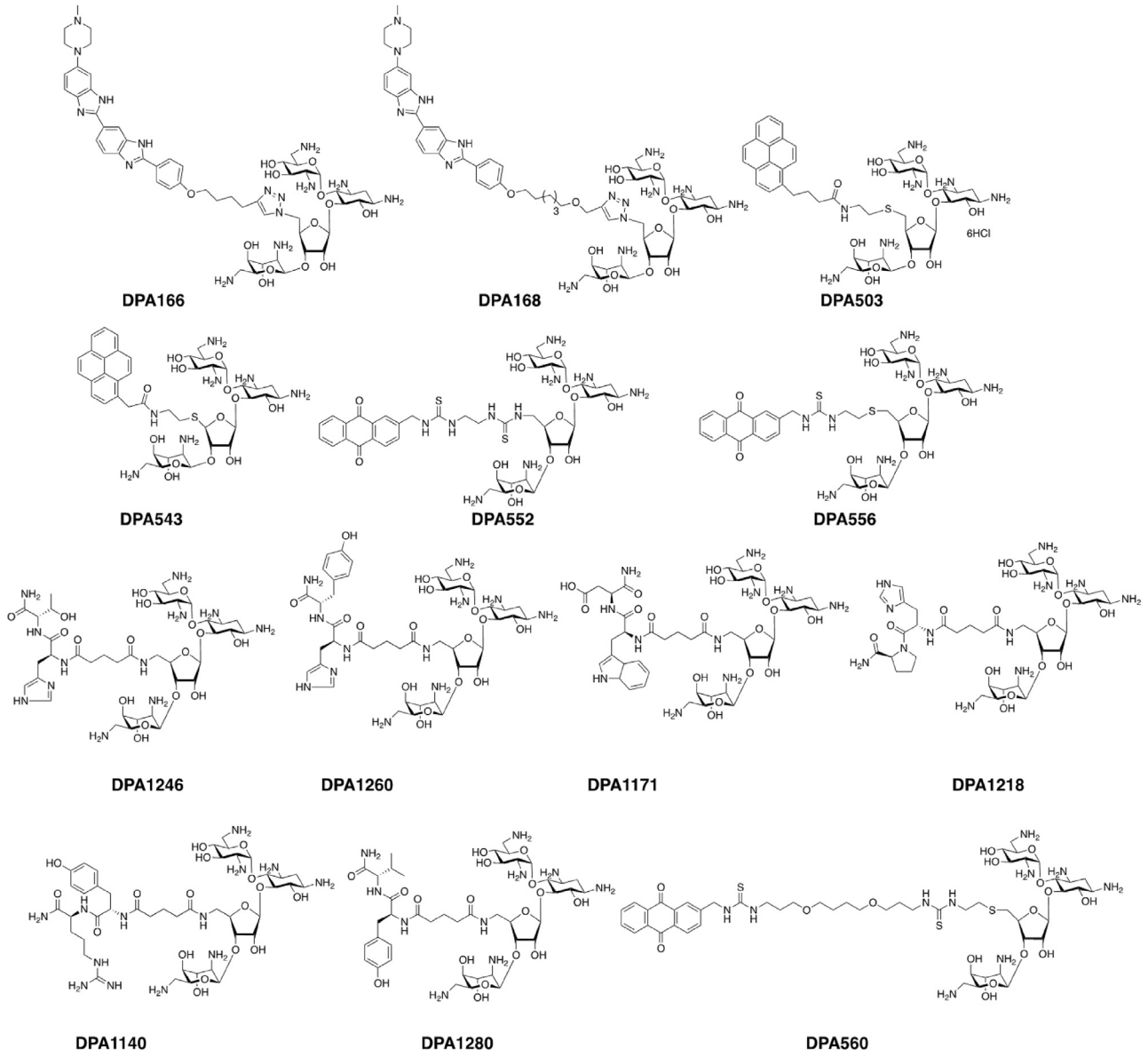

Figure 1. Structures of functionalized neomycin derivatives used in the study

miRs (Figure S1C) revealed around 25 miRs to be downregulated (Figure S1D). Although the heatmap indicates the extremely high expression of miR-21 compared with the other represented miRs, DPA 560 at 5 μM concentration was able to knock down its expression without causing any deleterious effect to the MCF-7 cells. To validate the miR profiling, we chose two other miRs, miR-96, which shows downregulation, and miR-155 on which DPA 560 did not have any effect, and checked their expression. qRT-PCR data showed downregulation of miR-96 upon DPA 560 treatment and non-significant change in its pre-miR levels. Mature and pre-miR-155 on the other hand showed inconsistent expression levels upon treatment with DPA 560. When DPA 560 dose-dependent treatment was administered to cells and both these miRs were tested, they displayed aberrant expression levels across all the concentrations, unlike miR-21 which had downregulated in a gradient manner upon dose-dependent DPA-560 treatment. We could therefore conclude that the aromatic-neomycin molecule DPA 560 targets miR-21 at a precursor stage, and inhibit its maturation, thereby reducing the mature transcript level within cells.

Determination of miR-21 cognate target protein (PTEN and PDCD4) expression levels after treatment with aromatic-neomycin molecules

miR-21 is known to target proteins, such as phosphatase and tensin homolog (PTEN) and Programmed cell death protein 4 (PDCD4).

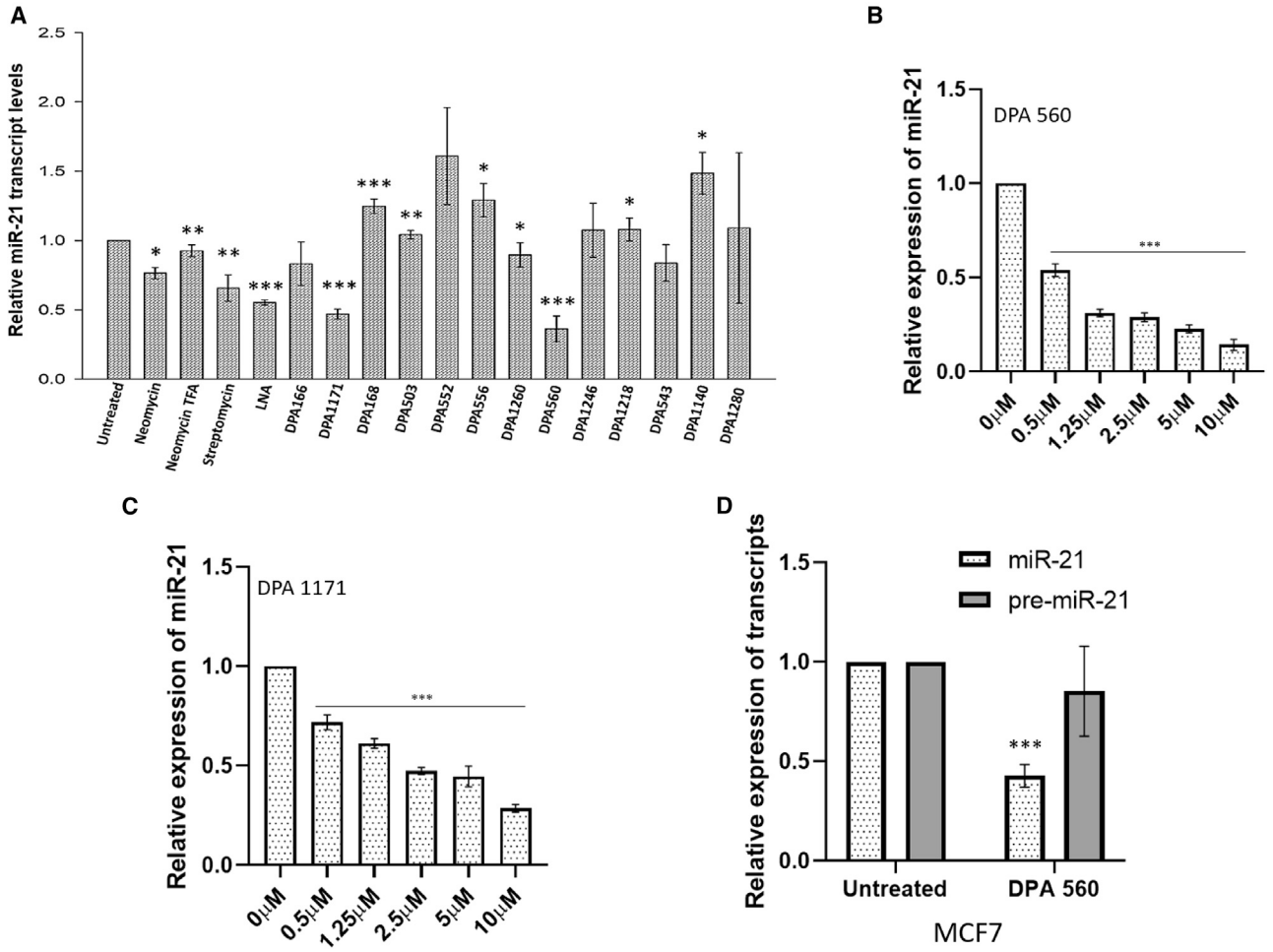

Figure 2. Aromatic-neomycin small molecules are effective in downregulating miR-21 transcript levels within cells

(A) Relative expression of miR-21 transcript levels in cells treated with aromatic-neomycin conjugates at 5 μM concentration compared with the control samples chosen, measured through qRT-PCR. (B) qRT-PCR to check relative miR-21 levels upon dose-dependent treatment of DPA 560 from 0 to 10 μM. (C) qRT-PCR to check relative miR-21 levels upon dose-dependent treatment of DPA 1171 from 0 to 10 μM. (D) qRT-PCR to check the relative expression of pre-miR-21 compared with mature miR-21 in MCF7 cells. (A–D) Samples were normalized to U6 RNA serving as an internal control. The data shown in the figure are representative of three biological replicates with error bars ± SD. *$p < 0.5$, **$p < 0.005$, ***$p < 0.001$; Student's t test.

PTEN and PDCD4 are proteins that both act as tumor suppressors as they regulate important cellular dynamics, such as apoptosis, proliferation, migration, and EMT. Due to elevated levels of onco-miR-21, they get suppressed thereby losing out on their tumor-suppressing activity. Treatment with aromatic-neomycin molecules already showed a reduction in the levels of mature miR-21 within MCF-7 cells and so we wanted to test whether these molecules were equally capable of reflecting this effect at the translational level. Treatment of aromatic-neomycin molecules at 5 μM concentration was administered to the cells and similar controls were used as stated in the previous study. After 48 h of treatment, western blot was performed to study the levels of both PTEN and PDCD4. For PTEN, DPA 560 and DPA 1171 both were able to elicit a major upregulation of the protein, with DPA 560 causing a 2-fold increase of PTEN expression relative to untreated cells (Figures 3A and 3B). Similar results were observed with PDCD4 (Figures S2A and S2B). For both the proteins, DPA 1171, although showing upregulation, the fold change was not as high as for DPA 560, which indicates that DPA 560 is more potent even at the translational landscape. To further establish the effect on PTEN and PDCD4 upregulation, we performed western blot to check both the protein levels post-DPA 560 treatment in an incremental concentration gradient. We observed PTEN and PDCD4 protein levels gradually went up as the concentration of treatment increased from 0 to 10 μM (Figures 3C 3D, S2C, and S2D). We further validated this effect on MCF-7 cells after 48 h of DPA 560 treatment by performing qRT-PCR to check the mRNA levels for PTEN and PDCD4 proteins. We found that both the transcripts showed an elevated level of 1.5- to 2-fold expression upon the molecule treatment when compared with the untreated cells (Figure S2E). Our results at the miR-21 target protein level and their respective transcriptional level strongly co-relate

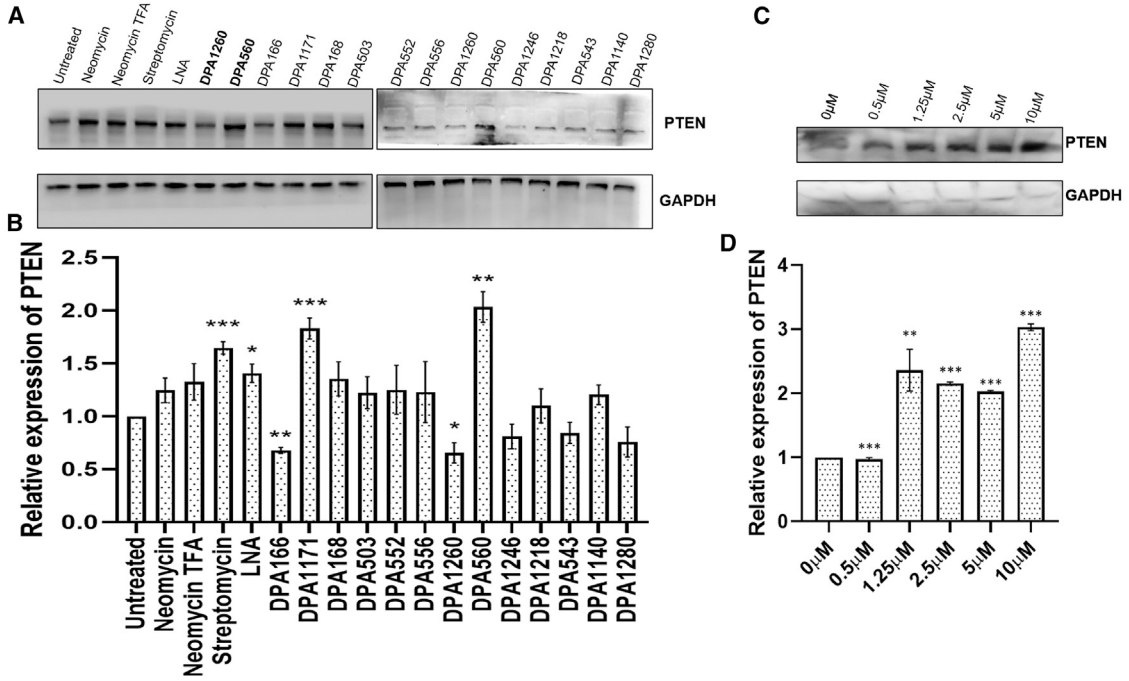

Figure 3. Treatment with aromatic-neomycin conjugates upregulates miR-21 target proteins *in cellulo*

(A) Data represent western blot for PTEN (target protein for miR21). Relative expression levels of PTEN for cells treated with aromatic-neomycin conjugates at 5 μM concentration compared with the control samples. The shared conditions between the two sets of blots are represented in bold on the right side of the blots. (B) Quantitative analysis of the prior blot via ImageJ denotes the most effective molecule to downregulate miR-21, thereby increasing PTEN levels. (C) Relative expression of PTEN protein represented by western blotting after dose-dependent treatment of DPA 560 from 0 to 10 μM. (D) Quantitative analysis of the prior blot via ImageJ shows an increment in PTEN protein levels upon an increase in DPA 560 treatment to cells. (A–D) Samples were normalized with the housekeeping gene GAPDH. The data shown in the figure are representative of three biological replicates with error bars ± SD. *p < 0.5, **p < 0.005, ***p < 0.001; Student's t test.

to the observation acquired at the miR level, further validating the study.

Binding affinity study of aromatic-neomycin conjugate and miR21

The binding analysis study was performed in Octet RED96 for selected aromatic-neomycin molecules DPA 560 and DPA 1171, which were the best hits obtained from previous experiments. Data obtained from qRT-PCR and western blot assays were further validated from this binding affinity study, yielding strong support for the role PAs play in hindering the maturation of miR-21. Binding association and dissociation patterns were observed (Figures 4 and S3) and the K_D value obtained for both molecules are tabulated in Table S1. Both the molecules showed a strong binding and minimal dissociation over the initial two concentrations but, upon increment, in the concentration, the dissociation fold change for DPA 1171 increased, as compared with DPA 560, which indicates that DPA 560 could bind to pre-miR-21 and inhibit the Dicer activity for a longer time. The K_D values as recorded for both molecules were comparable.

Cellular toxicity check of the most potent aromatic-neomycin molecule DPA 560

Treatment of small molecules can cause cellular toxicity due to the stress imposed upon cells by foreign material. Therefore, the correct dosage of treatment should be chosen at which the cells are viable. Cell viability is the percentage of living cells compared with dead cells in a particular condition. This was checked for DPA 560 by MTT assay where the 2.5–25 μM dosage range for treatment of molecules was chosen across which even the highest concentration showed a cell viability of ∼80% and, up to 10 μM of DPA 560 treatment, the cell viability was ∼90% (Figure S4). Therefore, this shows that the molecule used is non-toxic to cells.

Checking potential of aromatic-neomycin conjugate DPA 560 in checking cellular proliferation

From the previous studies, DPA 560 proved to be a prominent molecule that worked effectively across all the assays and therefore was further chosen to characterize the downstream effect of the protein pathways. Cellular proliferation is one of the mechanisms that PTEN and PDCD4 both regulate. Any aberration within cells when detected causes cell-cycle arrest and therefore a reduction in proliferation. Ki-67 is one of the most commonly used markers for proliferation. We wanted to check the proliferative potential of MCF-7 untreated cells in comparison with the DPA 560-treated cells, as well as in a condition where the miR-21 levels were rescued after treatment. So, we transfected *in vitro* synthesized pre-miR-21 in the cells immediately after treatment with DPA 560. To verify whether the miR-21 expression in the rescue was equivalent to the untreated cells,

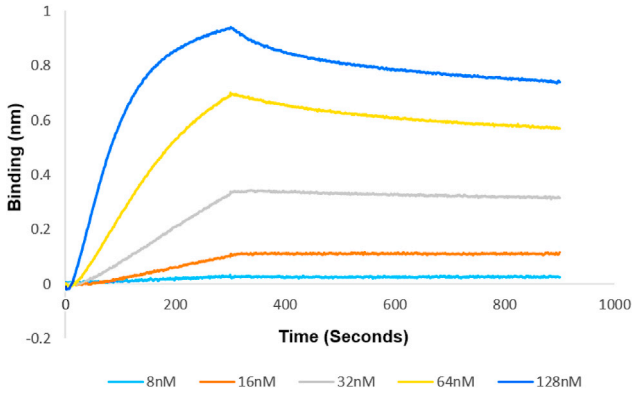

Figure 4. Binding affinity study of aromatic-neomycin conjugate and miR-21

Association and dissociation pattern for DPA 560 to pre-miR21 over the concentration range of 8–128 nM of DPA 560.

we performed qPCR to estimate the pre-miR-21 and miR-21 expression in untreated, DPA 560-treated, and miR-21 rescue cells. We found that the transfection of pre-miR-21 in the rescue condition enhanced its levels within cells to 1.5-fold, because of which the mature miR-21 levels were equivalent in this condition to that of untreated cells, despite the presence of DPA 560 molecules (Figure 5A). The DPA 560-treated cells showed downregulation of miR-21 and there was no change in the pre-miR-21 expression (Figure 5A). As it was now established that miR-21 levels could be rescued within cells, the immunofluorescence for Ki67 protein was performed for untreated, DPA 560-treated, and miR-21 rescue cells. In the untreated samples, we found bright foci all across the nucleus for Ki67, indicating that the cell was in its proliferative phase (Figures 5B and 5C). A similar effect was seen for cells treated with molecule DPA 503 (Figures 5B and 5C), which did not show any effect in our previous assays and so was chosen as a negative control. When we treated the same cells with DPA 560, we found the disappearance of the nuclear foci for Ki67, and only a faint outline of the nucleolus was visible (Figures 5B and 5C), and again when the *in vitro* synthesized pre-miR-21 was transfected in the DPA 560-treated cells to rescue miR-21 levels, they showed the presence of nuclear foci upon immunostaining with Ki67 antibody (Figures 5B and 5C). Also, to validate the effect of miR-21 downregulation due to DPA 560 treatment, followed by its rescue, we analyzed the cell cycle for the different conditions: untreated, DPA 560-treated, and miR-21 rescue cells (Figure S5A). Cells treated with DPA 560 show more populations of cells arrested at the G1 phase before transitioning to the S phase. This is due to the upregulation of the miR-21 target proteins PTEN and PDCD4, which are already reported to play a role in G1-S phase arrest. This effect was again reverted upon rescue of miR-21 levels and the cell population in each cell-cycle stage was similar to that of the untreated cells. We could, therefore, infer that DPA 560 is highly effective in reducing the miR-21 effect on transcriptional and translational grounds, and the potency is high enough to cause a check in cancer cell proliferation as well.

Cell migration and invasion check by aromatic-neomycin conjugate DPA 560 in breast cancer cell line

A classical characteristic of cancer progression in cells is via cell migration and invasion. An elevated level of miR-21 is one such factor that induces this phenomenon. Inhibition of miR21 can reduce the migratory behavior in cells. To establish DPA 560 as a potent molecule to suppress miR-21 and, thereby, reduce the deleterious downstream effects, we performed a wound-healing assay in MCF7 breast cancer cells. A scratch, made in fully confluent dishes under untreated, streptomycin, DPA 560-treated, and miR-21 rescue conditions was monitored at 0, 24, and 48 h. Indeed, the DPA 560-treated cells did not completely close up the wound in comparison with untreated, miR-21 rescue cells, and the streptomycin-treated positive control (Figure 5D). The same experiment was also performed in MDA-MB-231 cells, which is a more invasive breast cancer cell line, where we found the same effect of DPA 560 over untreated and streptomycin-treated cells up to 48 h (Figure S5B). Quantification of the wound exposure under all conditions in MCF7 cells revealed that, up to 48 h, 95% of wound area was still left uncovered in DPA 560-treated cells as compared with 40%–45% in streptomycin-treated cells, and ∼20%–25% in untreated and miR-21 rescue cells (Figure 5D). Similar results were obtained from the quantification of wound exposure in MDA-MB-231 cells for untreated, and DPA 560- and streptomycin-treated cells (Figure S5C). To consolidate this finding, we further performed a cell migration assay using transwell inserts. The MCF-7 cells in untreated, DPA 560-treated, and miR-21 rescue conditions were seeded in the transwell chambers, and after 48 h it was seen that the untreated and miR-21 rescue cells efficiently migrated across the basement membrane as compared with DPA 560-treated cells where the action was curbed (Figure 5F). Migratory cells also possess the ability to invade and penetrate nearby tissues, thereby colonizing new niches where tumor formation can take place. To check the invasion potential of MCF-7 cells, we performed an invasion assay in transwell inserts with the polycarbonate basement membrane, which the untreated and miR-21 rescue cells could breach, but the action was not prominent in the DPA 560-treated cells (Figure 5H). A quantitative estimate of the optical density of the stained migrated or invaded cells was performed. DPA 560-treated cells reduced up to 50% of both invasion and migration, in comparison with untreated or miR-21 rescue cells (Figures 5G and 5I). Thus, DPA 560 was quite effective in checking the migration and invasion potential of the cells by suppressing the miR-21 levels.

Efficacy of DPA 560 in inhibition of EMT phenomena in breast cancer cells

Metastasis is a process in cancer that happens at a later more progressive stage of the disease. It is due to this phenomenon that primary tumors enter into the blood circulation and disseminate into secondary or tertiary tumors. A major factor that drives this occurrence is EMT of the cells, where cells lose their adherence property and gain motility features. Some markers designate the onset of EMT, such as E-cadherin and vimentin. Multiple proteins are involved in triggering this process one of which is PTEN, which regulates this via the PI3K/Akt pathway inhibition. PI3K/Akt pathway augments the

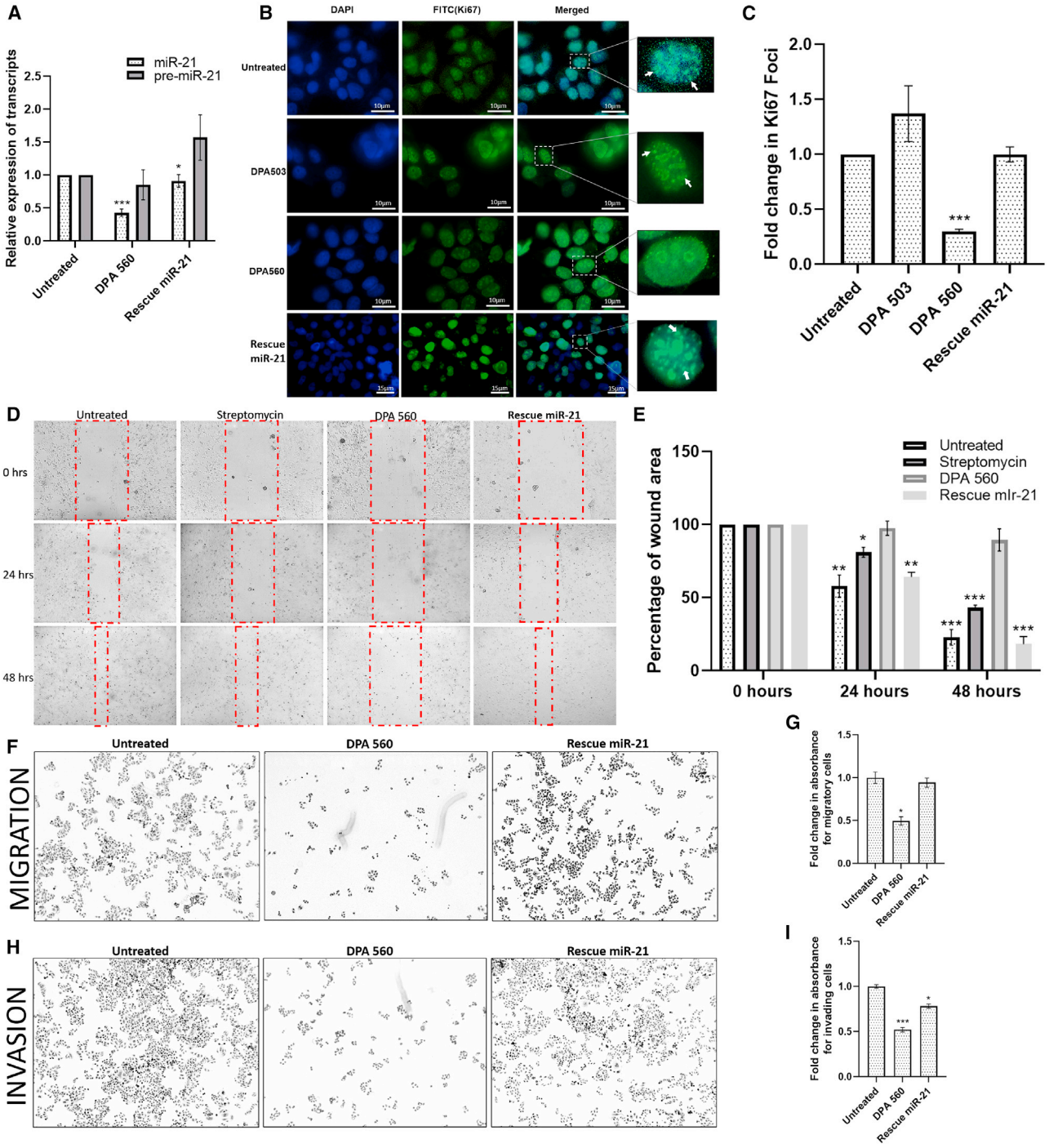

Figure 5. Aromatic-neomycin small-molecule DPA 560 curbs cellular proliferation, migration, and invasion in breast cancer cells

(A) qRT-PCR to check the relative expression of mature miR-21 and pre-miR-21 in untreated, DPA 560-treated, and miR-21 rescue MCF7 cells. Samples were normalized to U6 RNA serving as an internal control. The data shown in the figure are representative of three biological replicates with error bars ± SD. *p < 0.5, **p < 0.005, ***p < 0.001; Student's t test. (B) Representation of Ki67 cell proliferation assay showing foci within the cell nucleus as proof for the cells to be in the proliferative phase. The figure shows untreated cells, cells treated with DPA 503 (negative control), with DPA 560 (test hit), and cells rescued with miR-21. Scale bars for all the images are shown. The cells were viewed under 100× magnification (miR-21 rescue cells were imaged under 60× magnification). Magnified boxes from each image show the best-focused cell. (C) Quantification for the images is provided with error bars representing ± SD; *p < 0.05, **p < 0.005, ***p < 0.001; Student's t test. The data shown in the figure are representative of three biological replicates. (D) Wound-healing assay performed in MCF7 cells to monitor cell migration ability in untreated, streptomycin-treated, DPA 560-treated, and miR-

(legend continued on next page)

expression of the Snail transcription factor that negatively regulates epithelial marker E-cadherin which is a Ca^{2+}-dependent adhesion protein. miR-21 targets PTEN and suppresses it. This action boosts the PI3K/Akt pathway thereby promoting Snail followed by the onset of EMT and metastasis. From our previous assays, it was established that miR-21-dependent cell migration and invasion is curbed by the treatment of DPA 560 molecules. To prove its efficacy in inhibiting EMT, we therefore first checked the effect of DPA 560 treatment on Snail transcription factor expression by qRT-PCR. Downregulation of Snail after DPA 560 treatment established that PTEN upregulation after miR-21 knockdown might affect EMT status of the breast cancer cells (Figure 6A). We further validated this by checking the protein expression of Snail, along with phospho-Akt and pan-Akt. Western blot data showed significant downregulation in Snail and phospho-Akt levels while no change in the pan-Akt expression, thereby indicating the action of the molecules to inhibit EMT via the Snail-Akt axis (Figures 6B and 6C). We further proceeded to check the effect of DPA 560 small molecule on EMT markers within cells and whether it could mitigate cancer progression. E-Cadherin, which is an epithelial marker, and is useful for establishing cell-cell contact, was restored in our treated cells when compared with untreated cells (Figures 6D and 6E). High fluorescence intensity of E-cadherin expression localized to the cell membranes was observed in DPA 560-treated cells, which would facilitate cell-cell contact. Similarly, vimentin, which is a type III intermediate filament protein and a mesenchymal marker has low expression in MCF-7 cells but is seen scattered across the cytoplasm (as it marks the cytoskeleton of the cells) in the untreated cells (Figure 6F). The expression for this protein is reduced to more than 50% in DPA 560-treated cells (Figures 6F and 6G). To capture the effect of EMT more prominently, we chose a more invasive breast cancer cell line, MDA-MB-231, and performed immunofluorescence after treatment with DPA 560 for both E-cadherin and vimentin. As MDA-MB-231 is E-cadherin negative, we could not capture the protein expression in untreated cells, although, in DPA 560-treated cells, we found a slight increase in E-cadherin expression within cells (Figures S6A and S6B). Vimentin, on the other hand, has high expression in this cell line and, compared with untreated cells, we could find a stark reduction in the protein expression after DPA 560 treatment (Figures S6C and S6D). The levels of E-cadherin and vimentin were also validated in the treated and untreated cells via western blotting, in both MCF-7 and MDA-MB-231 cells. E-cadherin showed a reduction in treated cells in MCF7 (Figures 6H and 6I) and was undetectable in MDA-MB-231 (Figures S6E and S6F). Vimentin, on the other hand, showed a reduction in both the cells lines in the DPA 560-treated cells (Figures 6H, 6I, S6E, and S6F). Therefore, our studies reveal that DPA 560 actively represses miR-21 and it strongly affects reversal of EMT both in MCF7 and MDA-MB-231 cell lines.

DISCUSSION

miRs comprise a major part of non-coding RNAs that is responsible for controlling ~70% of cellular regulation and homeostasis. Research in the past decade has identified miRs that play a pivotal and multistep role toward tumor formation and metastases, although the entire mechanism behind its deregulation is not deciphered yet. Therefore, miRs are being harnessed for new therapeutic strategies where specific cancer-causing miRs can be targeted.[64,65] Small molecules are one such promising strategy that can decrease oncogenic miRs. Various research to develop approaches to enhance the specificity and affinity of these small molecules are being performed. In our study, we have developed peptide-conjugated amino sugar, which interacts with miR and regulates its maturation ultimately leading to inhibition of cancer progression. We have shown how this conjugation leads to profound changes in downregulating mature miR-21 levels in breast cancer cells. The levels of cognate target protein (PTEN and PDCD4) for miR-21 were also increased upon treatment with the most potent small molecule. The molecule also resulted in the reversal of EMT. This study highlights that the small molecules binding to miR-21 competitively inhibit Dicer and therefore affect the overall onco-miR maturation. Such high-throughput screening of novel synthesized small molecules opens new avenues for more focused drug design and provides optimistic leads toward cancer therapeutics.

MATERIALS AND METHODS

F-neo screening

Pre-miR21 5′UGUCGGGUAGCUUAUCAGACUGAUGUUGACU GUUGAAUCUCAUGGCAACACCAGUCGAUGGGCUGUCUGA CA was ordered from IDT (Coralville, IA). All experiments were performed in 10 mM phosphate buffer supplemented with 25 mM KCl and 0.05 mM EDTA (pH 6.5). Pre-miRs were slowly annealed using a heating block. Solutions of pre-miRs in 2× buffer were cooled from 75°C to 25°C at 1°C /min rate. First, the stoichiometry of F-neo binding to each pre-miR was determined as previously reported by us.[52,54] F-neo (100 nM) was titrated with increasing concentrations of pre-miRs using 96-well plates in triplicate. Plates were scanned using 485 nm excitation wavelength and 525 nm emission wavelength. The signal was collected on a TECAN M1000Pro plate reader. The

21 rescue conditions at 0, 24, and 48 h time points. (E) Quantitative analysis for the area of the exposed wound under the experimental conditions at 0, 24, and 48 h time points, analyzed using ImageJ. Error bars represent ± SD; *p < 0.05, **p < 0.005, ***p < 0.001; Student's t test. The data shown in the figure are representative of three biological replicates. (F) Representation of cells in untreated, DPA 560-treated, and miR-21 rescue conditions, which migrated through the transwell chambers and were imaged under 10× objective. (G) Fold change in the absorbance of the dye at 560 nm, extracted from the migratory cells in the transwell chamber denoting the comparison in the motility of the cells in untreated, DPA 560-treated, and miR-21-rescued cells. Error bars represent ± SD; *p < 0.05, **p < 0.005, ***p < 0.001; Student's t test. The data shown in the figure are representative of three biological replicates. (H) Representation of cells in untreated, DPA 560-treated, and miR-21 rescue conditions, which invaded through the transwell membrane and were imaged under 10× objective. (I) Fold change in the absorbance of the dye at 560 nm, extracted from the cells invading the transwell membrane denoting the comparison in invading potential of the cells in untreated, DPA 560-treated, and miR-21-rescued cells. Error bars represent ± SD; *p < 0.05, **p < 0.005, ***p < 0.001; Student's t test. The data shown in the figure are representative of three biological replicates.

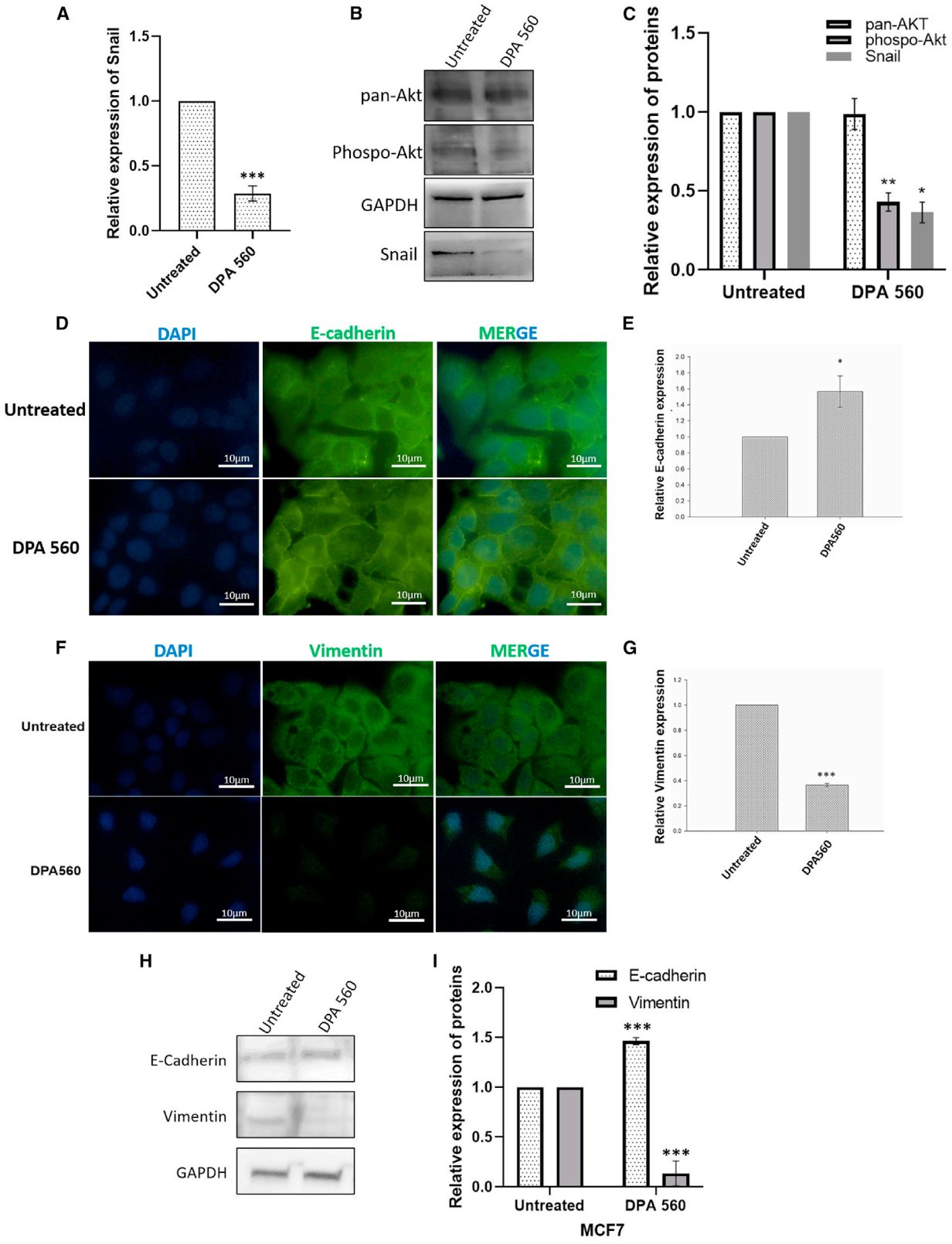

(legend on next page)

emission intensity of F-neo decreases as the concentration of RNA increases. Graphical analysis estimation of binding stoichiometry was 0.132 for pre-miR-21. It corresponds to 7.6 molecules of F-neo for one molecule of pre-miR-21. The pre-miR:F-neo complex was then titrated with neomycin or kanamycin to determine their IC_{50} values. IC_{50} is the concentration of a compound at which the intensity of F-neo emission is half of the maximum value. Pre-miRs were mixed with 100 nM F-neo at concentrations of 12.5 nM for pre-miR-21. Neomycin was serially diluted and its concentration varied from 2 μM to 0.9 nM after mixing with pre-miRs. IC_{50} values were measured in duplicate. The average IC_{50} value for neomycin was 42 ± 3 nM and the IC_{50} for kanamycin was ∼1,100 nM. Screening of pre-miR against neomycin conjugates was assessed using competition fluorescence assay at a single concentration of the added drug, as previously reported by us. Aromatic-neomycin compounds (peptide-neomycin library, pyrene, Hoechst, and anthraquinone conjugates) or neomycin were added at 100 nM concentration to the F-neo:RNA complex. Each plate contained duplicates of an F-neo:RNA complex without added compound and an F-neo:RNA complex with added 100 nM neomycin as a reference compound. Pre-miR-21 was mixed with 100 nM F-neo at 12.5 nM. Pre-miR-27a was mixed with 100 nM F-neo at 14.3 nM. The chosen ratio of F-neo [pre-miR] is based on binding stoichiometry. The top 13 compounds that showed the best binding were then chosen (Figure 1) for further analysis in cells.

Cell culture-treatments and transfections

MCF-7, MDA-MB-231 breast cancer cell line, and HeLa cells were chosen as the model system for the *in cellulo* experiments. The MCF-7 cell lines were purchased from ECACC, while the HeLa and MDA-MB-231 cells were obtained from the American Type Culture Collection and were maintained in DMEM (Dulbecco's modified Eagle's medium) medium (Gibco) with 10% FBS supplement (Gibco) and incubated at 37°C in an incubator with 5% CO_2. For experiments (RT-PCR and western blots) all the molecules (neomycin conjugates along with streptomycin as a positive control) were treated at a concentration of 5 μM. The experimental set had neomycin sulfate and neomycin TFA also as controls. Another positive control used in the experiments was antisense oligo for miR-21 (LNA), which was transfected in cells at a concentration of 50 nM. For rescuing the expression of miR-21, *in vitro* synthesized pre-miR-21 (with MEGAscript T7 IVT kit according to the manufacturer's manual) was transfected at 50 nM concentration. Lipofectamine 2000 (Invitrogen) was used as a transfection reagent. The transfection was done in 100% opti-MEM media (Gibco) and cells were incubated in it for 4–6 h, after which the medium was changed to complete DMEM. Cells were harvested for processing after 48 h for RNA and protein isolation.

RNA isolation, cDNA preparation, and qRT-PCR

After 48 h of treatment and transfection, total RNA isolation was done using TRIzol reagent from Ambion. DNase treatment was given to each sample for 30 min at 37°C to avoid DNA contamination. The enzyme was deactivated at 65°C for 10 min. The RNA acquired was then poly-adenylated by ATP using poly(A) polymerase and incubated at 37°C for 30 min. Next, to the poly-adenylated RNA, an oligoDT adaptor was added and incubated at 60°C for 5 min for annealing. After oligoDT annealing, reverse transcription was performed using RevertAid Reverse Transcriptase enzyme (Thermo Fisher Scientific) and the reaction mixture was incubated at 42°C for 1 h and enzyme deactivation was done at 95°C for 10 min. After the cDNA was prepared, qRT-PCR was performed for all treated samples in triplicate. The reaction volume for each well of the 384-well plate was 15 μL. The mature transcript level of miR-21, miR-96, and miR-155 were measured using the primers 5′-TAGCTTATCAGACTGATGTTGA-3′, 5′-TTTGGCACTAGCACATTTTTGCT-3′ and 5′-TTAATGCTAATCGTGATAGGGGTT-3′ respectively and as an internal control, U6 RNA transcript levels were measured using the primer 5′-CGCAAGGATGACACGCAAATTC-3′. To determine pre-miR levels within cells, cDNA was synthesized from the total RNA using stem-loop-specific primers for pre-miR-21, pre-miR-96, and pre-miR-155 using the QIAGEN cDNA synthesis kit and, further, their levels were checked by qPCR using the specific miR-21, miR-96, and miR-155 primers, respectively. For cDNA

Figure 6. DPA 560 is effective in the inhibition of EMT in breast cancer cells

(A) qRT-PCR to check the relative expression of Snail transcription factor in untreated cells and DPA 560-treated cells. Samples were normalized to the beta-actin housekeeping gene as an internal control. The data shown in the figure are representative of three biological replicates with error bars ± SD. *p < 0.5, **p < 0.005, ***p < 0.001; Student's t test. (B) Relative expression of proteins represented by western blotting for pan-Akt, phospho-Akt, and Snail, with GAPDH used as a housekeeping gene, in untreated and DPA 560-treated MCF7 cells. (C) Quantification of the prior blot performed by ImageJ to show a decrease in Snail and phospho-Akt protein while there was no change in the pan-Akt levels. Samples were normalized with the housekeeping gene GAPDH. The data shown in the figure are representative of three biological replicates with error bars ±SD. *p < 0.5, **p < 0.005, ***p < 0.001 (Student's t test) (D) Representation of images for EMT analysis done by immunofluorescence assay showing the comparative difference among the untreated cells and cells treated with DPA 560 for the E-cadherin marker in MCF7 cells. The cells were viewed under 100× magnification. (E) Quantification of the image (done by ImageJ) has been shown to demonstrate the effect of DPA 560 on the inhibition of EMT by an increase in the relative expression of the E-cadherin protein as compared with the control cells. The experiment has been done in three biological replicates. Figures for quantification show error bars representing ±SD. *p < 0.05, **p < 0.005, ***p < 0.001 (Student's t test). (F) Representation of images for EMT analysis done by immunofluorescence assay showing the comparative difference among the untreated cells and cells treated with DPA 560 for the vimentin marker in MCF7 cells. The cells were viewed under 100× magnification. (G) Quantification of the image (done by ImageJ) has been shown to demonstrate the effect of the DPA 560 on the inhibition of EMT by a decrease in the relative expression of vimentin as compared with the control cells. The experiment has been done in three biological replicates. Figures for quantification show error bars representing ±SD. *p < 0.05, **p < 0.005, ***p < 0.001 (Student's t test). (H) Relative expression of proteins represented by western blotting for E-cadherin and vimentin in untreated and DPA 560-treated MCF7 cells. (I) Quantification of the blot performed by ImageJ to show increase and decrease in E-cadherin and vimentin, respectively. Samples were normalized with the housekeeping gene GAPDH. The data shown in the figure are representative of three biological replicates with error bars ± SD. *p < 0.5, **p < 0.005, ***p < 0.001; Student's t test.

preparation for mRNA transcripts, random nonamers were used as provided in the QIAGEN cDNA synthesis kit. Transcript levels were determined using SYBR Green Master Mix-SYBR *Premix Ex Taq II* (Tli RNase H Plus) (from TaKaRa) in a Light Cycler 480 (Roche) instrument. Fold change analysis was done by the $2^{-\Delta\Delta Ct}$ method[66] across all the samples compared with untreated samples and internal control.

Small RNA sequencing and analysis

RNA isolated from untreated MCF-7 and DPA 560-treated MCF-7 cells were sequenced for small RNAs in duplicate. NEBNext Multiplex Small RNA Library Prep Kit was used to prepare the libraries for miR sequencing. The NEB adapters in this kit were directly, and specifically, ligated to miRs. The RNA 3′ adapter is specifically modified to target miRs and other miRs that have a 3′ hydroxyl group. The RT primers are annealed to the 3′ adapters to prevent adapter dimer formation. This is followed by the 5′ adapter ligation to the 5′-phosphate group of the small RNA molecules. Next, the RT reaction was used to create single-stranded cDNA. The cDNA was then PCR amplified using a common primer and a primer containing index sequences to generate final indexed libraries. These products were then selected on a gel to yield size-specific (140–160 bp) small RNA library. Prepared libraries were then sequenced on Illumina NextSeq 500 for 15M 75 bp SE reads. Up to 80% of the sequenced bases were of Q30 value. Sequenced data were processed to generate FASTQ files. Overall, 41,407,092 single-end reads were sequenced. The miRDeep2 package was used for 3′ adaptor removal, length-based filtering (minimum 16 nucleotides) followed by read alignment (Bowtie1) against the human reference genome from Gencode (GRCh38.p13) and miRBase (v.22). Differential expression analysis was performed using edgeR with quasi-likelihood F tests. Any miR showing raw read count <10 were excluded. Heatmap was generated by Bioconductor Complex Heatmap package. The sequencing files are submitted in the Sequence Read Archive database with accession number PRJNA748015 under submission ID SUB10035940. The table containing information on the 47 differentially expressed miRs is in the supplemental information, Table S2.

Western blot

After 48 h of treatment/transfection, cell medium was removed, washed with PBS, and then lysed using Cell Lytic lysis buffer (Sigma). The plates were incubated with the buffer and 1× protease inhibitor cocktail (Sigma) at 4°C on a rocker for 1–2 h. After incubation, the lysate was collected and centrifuged at full speed for 5 min to settle the cell debris. After centrifugation, the supernatant was collected, and protein estimation was done for all samples using a Pierce BCA Protein Assay Kit (Thermo Fisher). Equal concentrations of protein (40 μg) were measured for each sample and loaded on a 10% SDS-PAGE gel. After resolving the protein, they were transferred to a 0.2-μm PVDF membrane (GE Healthcare Life Science) from the gel. As the proteins were transferred, the blot was cut according to our desired protein size, and then blocked using 5% BSA (HiMedia). After successful blocking, the blots were incubated with the desired antibody (PTEN, PDCD4, pan-Akt, or GAPDH, purchased from Abcam; E-cadherin, vimentin, Snail, or p-AKT, purchased from CST) overnight at 4°C on a rocker. After incubation with primary antibody, blots were washed thrice, for 15 min each using 1× TBST. After washing, blots were incubated for 2 h with the respective HRP-conjugated secondary antibodies (anti-mouse/anti-rabbit). After secondary antibody incubation, a similar washing step was performed as before. After washing, blots were developed using EMD Millipore Immobilon Western Chemiluminescent HRP Substrate (ECL) in a Gel Doc instrument (Syngene). Quantification for the blots was done using ImageJ software.

Binding affinity studies

In vitro binding affinity studies were done using the Octet Red system from Forte Bio. The instrument is known to provide the most reliable kinetic parameters of binding and dissociation. Biotinylated pre-miR-21 was ordered from IDT and was immobilized on streptavidin-coated welled plates. The machine and software are high throughput, and several analytes across varied concentration ranges can be tested at one go using the instrument's 8-channeled plate system. For our experiment, each well contained a reaction volume of 200 μL. The pre-miR-21 was immobilized on the plates at a concentration of 25 mg/mL. The test molecules were used over a concentration range of 8–128 nM. The buffer used for the entire system was 10 mM HEPES, 50 mM NaCl, and 0.05% Tween 20, which was degassed and filtered. The regeneration buffer system is comprised of 50 mM NaOH and 1 M NaCl. The association parameter was set over a time frame of 5 min followed by a dissociation period of 10 min.

Cell viability assay

For the cell viability test, MTT (dimethyl thiazol diphenyl tetrazolium bromide) assay was performed. A total of 8,000 cells was plated on a 96-well plate and incubated for 24 h. After incubation, to the adhered cells, treatment was given for the test molecule and control at the concentrations of 0, 2.5, 5, 7.5, and 10 μM. Each concentration for individual molecules was tested in triplicate. Incubation of 24 h post-treatment was carried out and then 20 μL of medium was removed for addition of 20 μL of MTT (Sigma) (0.5 mg/mL concentration). After MTT application, cells were incubated for 4 h at 37°C in the incubator. After 4 h, the entire medium and MTT were removed and the formation of violet crystals was visible at the bottom of the wells. The violet crystals were dissolved using 150 μL of DMSO (Sigma). Absorbance was recorded using a TECAN plate reader at 570 nM. The percentage of viable cells was then calculated according to the manufacturer's recommendation.

Proliferation (Ki67) assay

MCF7 breast cancer cells were seeded at a density of 8×10^4 in a 6-well plate that already had pre-immersed Corning 22 mm^2 coverslips in each well to which cells had adhered. After adherence of the cells 24 h post-seeding, they were treated with aromatic-neomycin conjugates that were identified as hits from the qPCR and western blot experiments, and transfection of pre-miR-21 was also performed to obtain miR-21 rescue cells. After 48 h of treatment, the cells were washed with 1× PBS. Cells on the coverslips from the wells were then fixed using fixation buffer (3% paraformaldehyde, 5 μM EGTA [pH 8], 1 μM $MgCl_2$) for 10 min. After fixation, cells were

washed with washing buffer (30 μM glycine in PBS, 5 μM EGTA, and 10 μM $MgCl_2$) twice, and then permeabilized using permeabilization buffer (0.2% Triton X-100 in PBS, 5 μM EGTA, and 10 μM $MgCl_2$). After permeabilization, a similar washing step was followed. The wells containing the coverslips with adhered cells were next blocked using blocking buffer (0.5% BSA in PBS, 5 μM EGTA, 10 μM $MgCl_2$) for 30 min. After blocking was performed the cells were incubated overnight with primary antibody Ki67 (Abcam), which is a marker for proliferation, at a dilution of 1:1,000. Cells were washed thrice for 5 min each using blocking buffer post-incubation with primary antibody. This was followed by incubation with secondary antibody Alexa Fluor 488 (Invitrogen) (detected under the FITC filter) at 1:2,000 dilution for 2 h. After incubation with secondary antibody, cells were washed thrice for 5 min each using blocking buffer. In each well 600 μL of 1× PBS was added next, in which a drop of Prolong Gold Antifade Mountant with DAPI (Thermo Fisher) was added and incubated for 5 min. The coverslips then were mounted on a glass slide (Corning) and then viewed and analyzed using a Nikon Eclipse Ti-ε Inverted Microscope system (Epi-TIRF module) under 100× objective focus. Quantification for the images was done using ImageJ.

Cell-cycle analysis

Seeding of MCF-7 cells was done on 12-well plates and treatment of DPA 560 at 5 μM concentration was performed. Transfection of pre-miR-21 was also performed to obtain miR-21 rescue cells. At 48 h post-treatment and transfection, the cells were trypsinized, centrifuged, and washed with 1× PBS twice. This was followed by cell fixation in 70% ethanol overnight at −20°C. The pellet was resuspended in 200 μL of 4 mM sodium citrate buffer containing 0.1% Triton X-100 and RNase A at 100 μg/mL final concentration and incubated for 2 h at 37°C. Following incubation, cells were stained with propidium iodide at 30 μg/mL concentration and incubated at room temperature in the dark for 15–20 min. Cell-cycle analysis was carried out using a BD LSR flow cytometer.

Wound-healing assay

The wound-healing assay was performed using MCF7 and MDA-MB-231 breast cancer cells to understand the potential of the aromatic-neomycin hit molecules to curb the migration of cells. The cells were densely seeded in a 12-well plate so that, upon adherence, it reached full confluency. A vertical and horizontal wound was created on the plates after cell adherence, using a 200-μL pipette tip. The medium was discarded and the cells were washed thoroughly so that all non-adhered cells due to wound infliction were cleared off. After washing, the cells were given streptomycin and DPA 560 treatments at 5 μM concentration, transfection of pre-miR-21 was performed, and untreated cells were kept as control. Images were captured at 0, 24, and 48 h post-treatment using the phase-contrast module of an Evos FL Imaging system with a 4× magnification lens. After capturing images at each time point, the plates were kept in a humidified incubator at 37°C with 5% CO_2. The plates were discarded after the last time point at 48 h. Quantification of the images was performed using ImageJ software.

Transwell invasion and migration assay

Invasion and migration assay for MCF-7 breast cancer cells was done using a CytoSelect cell migration and invasion assay kit (Cell Biolabs) using the manufacturer's protocol. In brief, after 24 h of treatment/transfection, the cells were counted and placed on the transwell inserts at 100 cells/mL in FBS-free DMEM in complete medium and were allowed to migrate for 24 h at 37°C in humidified incubators. Non-migratory or non-invading cells from the top of the inserts were cleaned and the cells that migrated/invaded through the polycarbonate basement membrane were fixed, stained, and images were taken using an EVOS FL microscope under the 10× objective. The stained cells on the basement membrane were extracted and the optical density was recorded at 560 nm and quantified.

Assay to detect EMT

To check EMT for the treated and untreated cells, the protocol followed was similar to that followed for the proliferation assay, as described before. Cells were treated with aromatic-neomycin conjugates that delivered the best results from the assays performed previously. Untreated cells served as the control. Primary antibodies E-cadherin and vimentin (from Cell Signaling Technology) were used as markers for EMT and were used at a ratio of 1:500. The secondary antibody used was Alexa Fluor 488 (Invitrogen) (visible under the FITC range) at a 1:1,000 dilution. Quantification for the images was done using ImageJ.

Statistical methods

The statistical significance analysis for experiments was performed using Microsoft Office Excel and GraphPad Prism 8.0 across different replicates. All the data presented are mean ± SD of three independent biological replicate on which a two-tailed unpaired Student's t test was performed. The experiment data were considered significant with $p < 0.05$. *$p < 0.05$, **$p < 0.005$, and ***$p < 0.001$. Biological replicates used are similar to what is employed in the field.

SUPPLEMENTAL INFORMATION

Supplemental information can be found online at https://doi.org/10.1016/j.omtn.2021.12.027.

ACKNOWLEDGMENTS

We thank the National Institute of Health for financial support (grants GM097917, AI142856) to DPA. SM acknowledges financial support from the Council for Scientific and Industrial Research and the Department of Biotechnology Government of India (project MLP2104 GAP-0132)

AUTHOR CONTRIBUTIONS

A.G. performed all the biological assays mentioned in this study and wrote the paper. N.R., L.J., C.G., and N.D. were involved in the synthesis and characterization of the molecules. A.H.A. and S.A. assisted in the small RNA sequencing analysis. D.P.A. supervised the work performed at Clemson University and NUBAD. S.M. supervised the work conducted in CSIR-IGIB.

DECLARATION OF INTERESTS

D.P.A. has a financial interest in NUBAD LLC.

REFERENCES

1. Todua, F., Gagua, R., Maglakelidze, M., and Maglakelidze, D. (2015). Cancer incidence and mortality—major patterns in GLOBOCAN 2012, worldwide and Georgia. Bull. Georg. Natl. Acad. Sci. *9*, 168–173.
2. Mehlen, P., and Puisieux, A. (2006). Metastasis: a question of life or death. Nat. Rev. Cancer *6*, 449–458.
3. Monteiro, J., and Fodde, R. (2010). Cancer stemness and metastasis: therapeutic consequences and perspectives. Eur. J. Cancer *46*, 1198–1203.
4. Nguyen, D.X., and Massagué, J. (2007). Genetic determinants of cancer metastasis. Nat. Rev. Genet. *8*, 341–352.
5. Kalluri, R., and Weinberg, R.A. (2009). The basics of epithelial-mesenchymal transition. J. Clin. Invest. *119*, 1420–1428.
6. Kim, D., Xing, T., Yang, Z., Dudek, R., Lu, Q., and Chen, Y.-H. (2017). Epithelial mesenchymal transition in embryonic development, tissue repair and cancer: a comprehensive overview. J. Clin. Med. *7*, 1.
7. Thiery, J.P. (2002). Epithelial-mesenchymal transitions in tumour progression. Nat. Rev. Cancer *2*, 442–454.
8. Fidler, I.J. (2003). The pathogenesis of cancer metastasis: the 'seed and soil' hypothesis revisited. Nat. Rev. *3*, 453–458.
9. Park, S.M., Gaur, A.B., Lengyel, E., and Peter, M.E. (2008). The miR-200 family determines the epithelial phenotype of cancer cells by targeting the E-cadherin repressors ZEB1 and ZEB2. Genes Dev. *22*, 894–907.
10. Gregory, P.A., Bert, A.G., Paterson, E.L., Barry, S.C., Tsykin, A., Farshid, G., Vadas, M.A., Khew-Goodall, Y., and Goodall, G.J. (2008). The miR-200 family and miR-205 regulate epithelial to mesenchymal transition by targeting ZEB1 and SIP1. Nat. Cell Biol. *10*, 593–601.
11. Tavazoie, S.F., Alarcón, C., Oskarsson, T., Padua, D., Wang, Q., Bos, P.D., Gerald, W.L., and Massagué, J. (2008). Endogenous human microRNAs that suppress breast cancer metastasis. Nature *451*, 147–152.
12. Yan, L., Huang, X., Shao, Q., Huang, M., and Deng, L. (2008). MicroRNA miR-21 overexpression in human breast cancer is associated with advanced clinical stage, lymph node metastasis and patient poor prognosis. Cold Spring Harb. Lab. Press. *14*, 2348–2360.
13. Zhu, S., Wu, H., Wu, F., Nie, D., Sheng, S., and Mo, Y.Y. (2008). MicroRNA-21 targets tumor suppressor genes in invasion and metastasis. Cell Res. *18*, 350–359.
14. Ma, L., Teruya-Feldstein, J., and Weinberg, R.A. (2007). Tumour invasion and metastasis initiated by microRNA-10b in breast cancer. Nature *449*, 682–688.
15. Friedländer, M.R., Lizano, E., Houben, A.J., Bezdan, D., Báñez-Coronel, M., Kudla, G., Mateu-Huertas, E., Kagerbauer, B., González, J., Chen, K.C., et al. (2014). Evidence for the biogenesis of more than 1,000 novel human microRNAs. Genome Biol. *15*, R57.
16. Krol, J., Loedige, I., and Filipowicz, W. (2010). The widespread regulation of microRNA biogenesis, function and decay. Nat. Rev. Genet. *11*, 597–610.
17. Huntzinger, E., and Izaurralde, E. (2011). Gene silencing by microRNAs: contributions of translational repression and mRNA decay. Nat. Rev. Genet. *12*, 99–110.
18. Bartel, D.P. (2013). MicroRNAs: target recognition and regulatory functions. Cell *136*, 215–233.
19. Friedman, R.C., Farh, K.K.H., Burge, C.B., and Bartel, D.P. (2009). Most mammalian mRNAs are conserved targets of microRNAs. Genome Res. *19*, 92–105.
20. Calin, G.A., Liu, C.G., Sevignani, C., Ferracin, M., Felli, N., Dumitru, C.D., Shimizu, M., Cimmino, A., Zupo, S., Dono, M., et al. (2004). MicroRNA profiling reveals distinct signatures in B cell chronic lymphocytic leukemias. PNAS *101*, 11755–11760.
21. Su, Q., Lv, X.W., Sun, Y.H., Ye, Z.L., Kong, B.H., and Qin, Z.B. (2019). MicroRNA-494 inhibits the LRG1 expression to induce proliferation and migration of VECs in rats following myocardial infarction. Mol. Ther. Nucleic Acids *18*, 110–122.
22. Wehbe, N., Nasser, S.A., Pintus, G., Badran, A., Eid, A.H., and Baydoun, E. (2019). MicroRNAs in cardiac hypertrophy. Int. J. Mol. Sci. *20*, 4714.
23. Karolina, D.S., Armugam, A., Tavintharan, S., Wong, M.T.K., Lim, S.C., Sum, C.F., and Jeyaseelan, K. (2011). MicroRNA 144 impairs insulin signaling by inhibiting the expression of insulin receptor substrate 1 in type 2 diabetes mellitus. PLoS One *6*, e22839.
24. Muhonen, P., and Holthofer, H. (2009). Epigenetic and microRNA-mediated regulation in diabetes. Nephrol. Dial. Transpl. *24*, 1088–1096.
25. Maes, O., Chertkow, H., Wang, E., and Schipper, H. (2009). MicroRNA: implications for Alzheimer disease and other human CNS disorders. Curr. Genomics *10*, 154–168.
26. Cui, L., Li, Y., Ma, G., Wang, Y., Cai, Y., Liu, S., Chen, Y., Li, J., Xie, Y., Liu, G., et al. (2014). A functional polymorphism in the promoter region of microRNA-146a is associated with the risk of Alzheimer disease and the rate of cognitive decline in patients. PLoS One *9*, e89019.
27. Xue, F., Zhu, L., Liu, S., Liu, W., Yang, C., Wang, L., and Cai, L. (2017). Long noncoding RNA ADAMTS9-AS2 is regulated by DNA methyltransferase 1 and inhibits the malignant behaviors of non-small cell lung cancer cells. Int. J. Clin. Exp. Pathol. *10*, 2599–2608.
28. Gupta, A., Swaminathan, G., Martin-Garcia, J., and Navas-Marti, S. (2012). MicroRNAs, hepatitis C virus, and HCV/HIV-1 co-infection: new insights in pathogenesis and therapy. Viruses *4*, 2485–2513.
29. Carter, J.V., Galbraith, N.J., Yang, D., Burton, J.F., Walker, S.P., and Galandiuk, S. (2017). Blood-based microRNAs as biomarkers for the diagnosis of colorectal cancer: a systematic review and meta-analysis. Br. J. Cancer *116*, 762–774.
30. Zhang, L., Huang, P., Li, Q., Wang, D., and Xu, C.X. (2019). miR-134-5p promotes stage I lung adenocarcinoma metastasis and chemoresistance by targeting DAB2. Mol. Ther. Nucleic Acids *18*, 627–637.
31. Ji, R., Zhang, X., Gu, H., Ma, J., Wen, X., Zhou, J., Qian, H., Xu, W., Qian, J., and Lin, J. (2019). miR-374a-5p: a new target for diagnosis and drug resistance therapy in gastric cancer. Mol. Ther. Nucleic Acids *18*, 320–331.
32. Esquela-Kerscher, A., and Slack, F.J. (2006). Oncomirs—microRNAs with a role in cancer. Nat. Rev. Cancer *6*, 259–269.
33. Xu, F., Yan, J.J., Gan, Y., Chang, Y., Wang, H.L., He, X.X., and Zhao, Q. (2019). miR-885-5p negatively regulates Warburg effect by silencing hexokinase 2 in liver cancer. Mol. Ther. Nucleic Acids *18*, 308–319.
34. Wa, Q., Huang, S., Pan, J., Tang, Y., He, S., Fu, X., Peng, X., Chen, X., Yang, C., Ren, D., et al. (2019). miR-204-5p represses bone metastasis via inactivating NF-κB signaling in prostate cancer. Mol. Ther. Nucleic Acids *18*, 567–579.
35. Ghosh, A., Ekka, M.,K., Tawani, A., Kumar, A., Chakraborty, D., and Maiti, S. (2019). Restoration of miRNA-149 expression by TmPyP4 induced unfolding of quadruplex within its precursor. Biochemistry *58*, 514–525.
36. Rufino-Palomares, E.E., Reyes-Zurita, F.J., Lupiáñez, J.A., and Medina, P.P. (2013). MicroRNAs as oncogenes and tumor suppressors. MicroRNAs Med. *302*, 223–243.
37. Medina, P.P., Nolde, M., and Slack, F.J. (2010). OncomiR addiction in an in vivo model of microRNA-21-induced pre-B-cell lymphoma. Nature *467*, 86–90.
38. Folini, M., Gandelini, P., Longoni, N., Profumo, V., Callari, M., Pennati, M., Colecchia, M., Supino, R., Veneroni, S., Salvioni, R., et al. (2010). miR-21: an oncomir on strike in prostate cancer. Mol. Cancer *9*, 1–12.
39. Feng, Y.,H., and Tsao, C.,J. (2016). Emerging role of microRNA-21 in cancer. Biomed. Rep. *5*, 395–402.
40. Zhang, C., Liu, K., Li, T., Fang, J., Ding, Y., Sun, L., Tu, T., Jiang, X., Du, S., Hu, J., et al. (2016). MiR-21: a gene of dual regulation in breast cancer. Int. J. Oncol. *48*, 161–172.
41. Asangani, I.A., Rasheed, S.A.K., Nikolova, D.A., Leupold, J.H., Colburn, N.H., Post, S., and Allgayer, H. (2008). MicroRNA-21 (miR-21) post-transcriptionally downregulates tumor suppressor Pdcd4 and stimulates invasion, intravasation and metastasis in colorectal cancer. Oncogene *27*, 2128–2136.
42. Mabuchi, Y., Yamoto, M., Minami, S., and Umesaki, N. (2006). Immunohistochemical localization of inhibin and activin subunits, activin receptors, and Smads in ovarian clear cell adenocarcinoma. Oncol. Rep. *15*, 291–296.
43. Zucchini-Pascal, N., Peyre, L., and Rahmani, R. (2013). Crosstalk between beta-catenin and snail in the induction of epithelial to mesenchymal transition in hepatocarcinoma: role of the ERK1/2 pathway. Int. J. Mol. Sci. *14*, 20768–20792.

44. Han, M., Wang, Y., Liu, M., Bi, X., Bao, J., Zeng, N., Zhu, Z., Mo, Z., Wu, C., and Chen, X. (2012). MiR-21 regulates epithelial-mesenchymal transition phenotype and hypoxia-inducible factor-1α expression in third-sphere forming breast cancer stem cell-like cells. Cancer Sci. *103*, 1058–1064.

45. Chan, S., and Wang, L. (2015). Regulation of cancer metastasis by microRNAs. J. Biomed. Sci. *22*, 9.

46. Zhang, J., and Ma, L. (2012). MicroRNA control of epithelial-mesenchymal transition and metastasis. Cancer Metastasis Rev. *31*, 653–662.

47. Stenvang, J., Petri, A., Lindow, M., Obad, S., and Kauppinen, S. (2012). Inhibition of microRNA function by antimiR oligonucleotides. Silence *3*, 1.

48. Nahar, S., Singh, A., Morihiro, K., Moai, Y., Kodama, T., Obika, S., and Maiti, S. (2016). Systematic evaluation of biophysical and functional characteristics of seleno-methylene-locked nucleic acid-mediated inhibition of miR-21. Biochemistry *55*, 7023–7032.

49. Wen, D., Danquah, M., Chaudhary, A.K., and Mahato, R.I. (2015). Small molecules targeting microRNA for cancer therapy: promises and obstacles. J. Control Release *219*, 237–247.

50. Charles, I., and Arya, D.P. (2005). Synthesis of neomycin-DNA/peptide nucleic acid conjugates. J. Carbohydr. Chem. *24*, 145–160.

51. Gebert, L.F.R., Rebhan, M.A.E., Crivelli, S.E.M., Denzler, R., Stoffel, M., and Hall, J. (2014). Miravirsen (SPC3649) can inhibit the biogenesis of miR-122. Nucleic Acids Res. *42*, 609–621.

52. Ghosh, A., Degyatoreva, N., Kukielski, C., Story, S., Bhaduri, S., Maiti, K., Nahar, S., Ray, A., Arya, D.P., and Maiti, S. (2018). Targeting miRNA by tunable small molecule binders: peptidic aminosugar mediated interference in miR-21 biogenesis reverts epithelial to mesenchymal transition. Medchemcomm. *9*, 1147–1154.

53. Nahar, S., Ranjan, N., Ray, A., Arya, D.P., and Maiti, S. (2015). Potent inhibition of miR-27a by neomycin-bisbenzimidazole conjugates. Chem. Sci. *6*, 5837–5846.

54. Watkins, D., Jiang, L., Nahar, S., Maiti, S., and Arya, D.P. (2015). A pH sensitive high-throughput assay for miRNA binding of a peptide-aminoglycoside (PA) library. PLoS One *10*, 1–23.

55. Jiang, L., Watkins, D., Jin, Y., Gong, C., King, A., Washington, A.Z., Green, K.D., Garneau-Tsodikova, S., Oyelere, A.K., and Arya, D.P. (2015). Rapid synthesis, RNA binding, and antibacterial screening of a peptidic-aminosugar (PA) library. ACS Chem. Biol. *10*, 1278–1289.

56. Kumar, S., Ranjan, N., Kellish, P., Gong, C., Watkins, D., and Arya, D.P. (2016). Multivalency in the recognition and antagonism of a HIV TAR RNA-TAT assembly using an aminoglycoside benzimidazole scaffold. Org. Biomol. Chem. *14*, 2052–2056.

57. Watkins, D., Norris, F.A., Kumar, S., and Arya, D.P. (2013). A fluorescence-based screen for ribosome binding antibiotics. Anal. Biochem. *434*, 300–307.

58. Ranjan, N., and Arya, D.P. (2019). A Fluorescent Aminosugar to Rapidly Screen and Study RNA Binders, First edition (Elsevier Inc.).

59. Theng, B.K.G. (2012). Chapter 9. Nucleic acids. Dev. Clay Sci. *4*, 319–337.

60. Willis, B., and Arya, D.P. (2014). Recognition of RNA duplex by a neomycin-Hoechst 33258 conjugate. Bioorg. Med. Chem. *22*, 2327–2332.

61. Watkins, D., Gong, C., Kellish, P., and Arya, D.P. (2017). Probing A-form DNA: a fluorescent aminosugar probe and dual recognition by anthraquinone-neomycin conjugates. Bioorg. Med. Chem. *25*, 1309–1319.

62. Watkins, D., Kumar, S., Green, K.D., Arya, D.P., and Garneau-Tsodikova, S. (2015). Influence of linker length and composition on enzymatic activity and ribosomal binding of neomycin dimers. Antimicrob. Agents Chemother. *59*, 3899–3905.

63. Story, S., Skriba, M.J., Maiti, K., Ranjan, Nihar, Degtyareva, N.N., Green, K.D., Khodaverdian, V., Oyelere, A.K., Garneau-Tsodikova, S., and Arya, D.P. (2019). Synthesis, antimicrobial activity, attenuation of aminoglycoside resistance in MRSA, and ribosomal A-site binding of pyrene-neomycin conjugates. Eur. J. Med. Chem. *163*, 381–393.

64. Gasparello, J., Lomazzi, M., Papi, C., D'Aversa, E., Sansone, F., Casnati, A., Donofrio, G., Gambari, R., and Finotti, A. (2019). Efficient delivery of MicroRNA and AntimiRNA molecules using an argininocalix4arene macrocycle. Mol. Ther. Nucleic Acids *18*, 748–763.

65. Chakraborty, C., Sharma, A.R., Sharma, G., Doss, C.G.P., and Lee, S.S. (2017). Therapeutic miRNA and siRNA: moving from bench to clinic as next generation medicine. Mol. Ther. Nucleic Acids *8*, 132–143.

66. Livak, K.J., and Schmittgen, T.D. (2001). Analysis of relative gene expression data using real-time quantitative PCR and the $2^{-\Delta\Delta CT}$ method. Methods *25*, 402–408.